Tumbling Dynamics of Passive Flexible Wings

Daniel Tam* and John W. M. Bush
Department of Mathematics, Massachusetts Institute of Technology, Cambridge, Massachusetts 02139, USA

Michael Robitaille and Arshad Kudrolli
Department of Physics, Clark University, Worcester, Massachusetts 01610, USA

(Received 15 July 2009; revised manuscript received 6 April 2010; published 6 May 2010)

The influence of flexibility on the flight of autorotating winged seedpods is examined through an experimental investigation of tumbling rectangular paper strips freely falling in air. Our results suggest the existence of a critical length above which the wing bends. We develop a theoretical model that demonstrates that this buckling is prompted by inertial forces associated with the tumbling motion, and yields a buckling criterion consistent with that observed. We further develop a reduced model for the flight dynamics of flexible tumbling wings that illustrates the effect of aeroelastic coupling on flight characteristics and rationalizes experimentally observed variations in the wing's falling speed and range.

DOI: 10.1103/PhysRevLett.104.184504 PACS numbers: 47.85.−g, 46.32.+x, 46.40.Jj

Seed dispersal is the means by which plants expand and colonize new areas [1]. To maximize their range, some plants have developed elaborate gliding, spinning, or tumbling winged seedpods, whose aerodynamics enable them to extend their flight time and range [2]. Such winged seedpods are often light and thin, which generally decreases their surface loading and hence their rate of descent. As a consequence, they can be flexible, as demonstrated by the gliding seeds of *Alsomitra macrocarpa*, that deform substantially during flight. We are broadly interested in elucidating the role of flexibility in passive flight. Here, we focus on tumbling wings, such as the winged seedpods of *Ailanthus altissima*, and investigate the influence of flexibility on the tumbling dynamics.

Consider a rectangular wing of uniform thickness h, width w, cross-sectional area $A = wh$, length L, density ρ_s, bending stiffness EI, falling through air of density ρ under the influence of gravity $\mathbf{g}$. Studies of the dynamics of freely falling rigid wings have a rich history dating back to Maxwell [3]. Recent work has mainly focused on the transition between the fluttering and tumbling modes, which occurs at a critical value of $I_0 = \rho_s h/\rho w$ [4–6]. For small values of I_0, the wing oscillates in a side-to-side fluttering motion. Above a critical I_0, the wing tumbles, completing full rotations about its long axis, while drifting along an inclined trajectory [Fig. 1(b)]. The flight properties of tumbling rigid wings have been characterized extensively through experiments [7,8].

We investigated the influence of flexibility on passive tumbling flight experimentally using rectangular paper strips of varying surface density $\rho_s h$ and stiffness, namely, light, medium, and stiff paper with $\rho_s h = 6.0$, 7.5, 14×10^{-2} kg m^{-2} and bending moduli of $Eh^3/12 = 1.0$, 3.6, 29.2×10^{-4} kg m^2 s^{-2}, respectively. Paper wings of moderate to high aspect ratio, $L/w = 3$–30, were used by varying their length and width over the respective ranges $L = 5$–28 cm and $w = 0.5$–5 cm. The wings are released from an electromagnetic clamp with their leading edge parallel to the ground. Upon release, the rectangular wings promptly start tumbling at a high and constant rotation rate, a regime well beyond the fluttering-tumbling transition [5,6]. Trajectories are captured by a high-speed camera filming at 250 fps and recorded from either the front or side in order to extract the bending deflection amplitude Z, the rotation rate $\dot{\alpha}$, linear velocity U_G, and the angle of descent ϕ between the velocity vector $\mathbf{U}_G$ and the vertical [Fig. 1(a)]. These flight characteristics ranged from $Z \sim 0$–5 cm, $\dot{\alpha} \sim 20$–150 s^{-1}, $U_G \sim 0.7$–1.1 m/s, and $\phi \sim 50°$–30°. Short tumbling wings remain straight [Fig. 1(b)]; however, sufficiently long wings bend symmetrically, sagging about their center line [Fig. 1(c)]. While

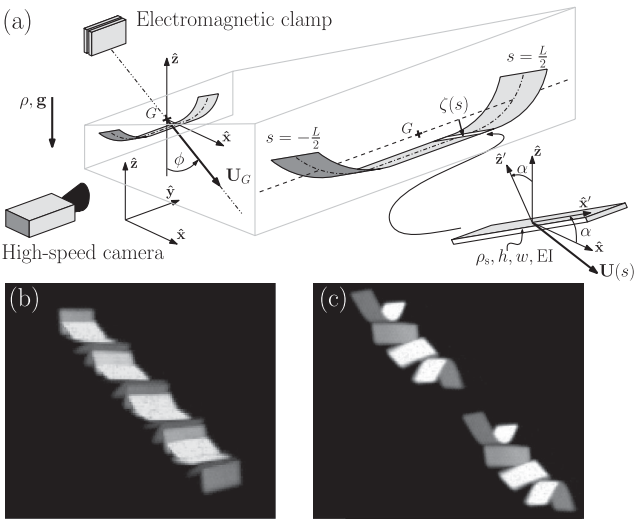

FIG. 1. (a) Schematic of the geometry of a falling, tumbling, bent wing. Superimposed snapshots of a tumbling paper wing: short wings remain straight (b), while long wings bend (c). For the sake of clarity, two half cycles are shown in (c) and images are artificially spaced. (See videos [11].)

previously reported [7,8], this bending remains unexplained. We observe the transition between the two regimes to be sharp as L is increased and to depend strongly on w and h. Throughout the motion, the deflection amplitude Z and rotation rate $\dot{\alpha}$ remain nearly constant. Specifically, fluctuations of no more than 15% are observed in either Z or $\dot{\alpha}$, with these maxima arising for the longest ($L > 25$ cm) and widest ($w > 3$ cm) wings. We here demonstrate that the wing buckles under the influence of inertia at a critical value of the transition parameter $\kappa = \sqrt[4]{\rho_s A \dot{\alpha}^2 / EI} L$, which prescribes the relative magnitudes of the destabilizing inertial force and the wing's elastic resistance to bending. We then elucidate the manner in which elastic deformation affects the tumbling dynamics.

We proceed by identifying the driving force behind the bending of a tumbling wing. The wing tumbles about the horizontal $\hat{\mathbf{y}}$ axis and the trajectories remain in the $(\hat{\mathbf{x}}, \hat{\mathbf{z}})$ plane. Since the bending moment of inertia is smallest in the cord direction $\hat{\mathbf{x}}'$, we assume bending to occur solely in the $(\hat{\mathbf{y}}, \hat{\mathbf{z}}')$ plane corotating with the wing, in accord with our observations (Fig. 1). The wing orientation is prescribed by the pitch angle α between the horizontal $\hat{\mathbf{x}}$ and cord direction $\hat{\mathbf{x}}'$. The position along the center line is given by the arc length s, and $\zeta(s)$ denotes the deflection at s in the $\hat{\mathbf{z}}'$ direction and measured from a line of direction $\hat{\mathbf{y}}$ through the center of gravity G. Hence the local velocity of the wing at the center line $\mathbf{U}(s)$ can be written $\mathbf{U}(s) = \mathbf{U}_G - \dot{\alpha}\zeta(s)\hat{\mathbf{x}}'$. All equations of motion are expressed in the corotating reference frame $(\hat{\mathbf{x}}', \hat{\mathbf{y}}, \hat{\mathbf{z}}')$.

For small deflections, bending deformation of the free wing is governed by the linear Euler-Bernoulli equations

$$\zeta_{ssss} - \frac{\mathbf{p} \cdot \hat{\mathbf{z}}'}{EI} = 0, \tag{1}$$

with free end boundary conditions $\zeta_{ss} = 0$ and $\zeta_{sss} = 0$ at $s = \pm L/2$. $\mathbf{p}$ is the force distribution per unit length along the wing and has three components: inertial, aerodynamic, and gravitational forces. It can be written $\mathbf{p}(s) = -\rho_s A \dot{\mathbf{U}}(s) + \mathbf{L}(s) + \mathbf{D}(s) + \rho_s A \mathbf{g}$, with $\mathbf{L}(s)$ and $\mathbf{D}(s)$ the local lift and drag. Newton's second law for the wing requires that $\int_{-L/2}^{L/2} \rho_s A \dot{\mathbf{U}} ds = \int_{-L/2}^{L/2} (\mathbf{L} + \mathbf{D} + \rho_s A \mathbf{g}) ds$, which we simply write as $\int_{-L/2}^{L/2} \mathbf{p}(s) ds = 0$. Consequently, a simple expression for the forcing $\mathbf{p}$ can be derived. Consider a wing tumbling in the straight configuration $\zeta(s) = 0$. In this case, $\mathbf{U}$ is constant along the span of the wing, so inertial forces are independent of s. Furthermore, for sufficiently long wings, three-dimensional aerodynamic effects at the wing tips can be neglected and the flow considered two-dimensional, in which case $\mathbf{L}$ and $\mathbf{D}$ are both independent of s. As a consequence, $\mathbf{p}$ is independent of s and so must indeed vanish to satisfy the conservation of linear momentum. Hence, we can deduce that the straight configuration $\zeta(s) = 0$ is always a solution, albeit a potentially unstable one.

Let us now consider a bent wing, whose small deflection ζ is constant in time, in accord with experimental observations. We seek to find the first order correction to $\mathbf{p}$ caused by finite bending ζ. The local inertial force at s now has an additional component $\rho_s A \dot{\alpha}^2 \zeta(s) \hat{\mathbf{z}}'$. Furthermore, given that the Reynolds number in our experiments $\mathrm{Re} = \rho w U_G / \mu$ is of order 10^3–10^4, the aerodynamic pressure scales as $\rho U(s)^2$ and the first order correction in ζ to the aerodynamic force now scales as $\rho w \dot{\alpha} U_G \zeta(s)$. The ratio of this first order correction in inertial forces to aerodynamic forces is large in our experiments: $\rho_s h \dot{\alpha} / \rho U_G > 10^2$, which allows us to neglect the aerodynamic contribution to the correction term and consider only an inertial forcing $\mathbf{p}(s) = \rho_s A \dot{\alpha}^2 \zeta(s) \hat{\mathbf{z}}'$.

The equation governing the bending dynamics (1) together with the inertial forcing forms an eigenvalue problem previously investigated in the context of fast spinning ballistic objects [9] and is similar to that arising in the Euler buckling of a beam under normal compression [10]. The solution to the ordinary differential equation (ODE) (1) is a linear combination of trigonometric and hyperbolic functions. For small values of the transition parameter $\kappa = \sqrt[4]{\rho_s A \dot{\alpha}^2 / EI} L$, the straight configuration, $\zeta(s) = 0$, is the only solution. However, when κ reaches a critical value corresponding to the eigenvalue condition

$$\tan\frac{\kappa}{2} = \pm \tanh\frac{\kappa}{2} \tag{2}$$

obtained from the boundary conditions, the existence of a nontrivial solution implies that the straight configuration becomes unstable to a bent configuration through an inertial buckling transition (see detailed derivation in [11]).

The onset of instability corresponds to the smallest κ satisfying Eq. (2), specifically $\kappa_\star \approx 4.73$. $\kappa_\star$ characterizes either a critical buckling length for a given rotation rate, or alternatively a critical buckling rotation rate for a given length. Note that the critical rotation rate corresponds precisely to the lowest natural frequency oscillation of a free beam. The nontrivial solution to Eq. (1) at the transition is symmetrical and can be written

$$\zeta(s) = Z \frac{\cos(\frac{\kappa_\star}{2}) \cosh(\frac{\kappa_\star}{L} s) + \cosh(\frac{\kappa_\star}{2}) \cos(\frac{\kappa_\star}{L} s)}{\cos(\frac{\kappa_\star}{2}) + \cosh(\frac{\kappa_\star}{2}) - 2\cos(\frac{\kappa_\star}{2}) \cosh(\frac{\kappa_\star}{2})}. \tag{3}$$

$Z = \zeta(0) - \zeta(L/2)$ is the deflection amplitude and remains undetermined from the linearized equation (1). As for Euler buckling, Eq. (1) precisely predicts the transition, but leaves undetermined the details of the deflection after the transition. Nevertheless, exact shapes can be computed by solving numerically the nonlinear bending equations using the MATLAB BVP4C routine (see detail in [11]). Numerically computed shapes are reproduced in Fig. 2(a). Note that higher order instabilities can theoretically arise for larger values of κ; however, such high values were not achieved experimentally. For each wing, both the normalized deflection Z/L and transition parameter κ can be estimated from recordings of free falling wings. The experimental data are reported in Fig. 2(c). The deflection Z is zero for small κ but increases sharply close to

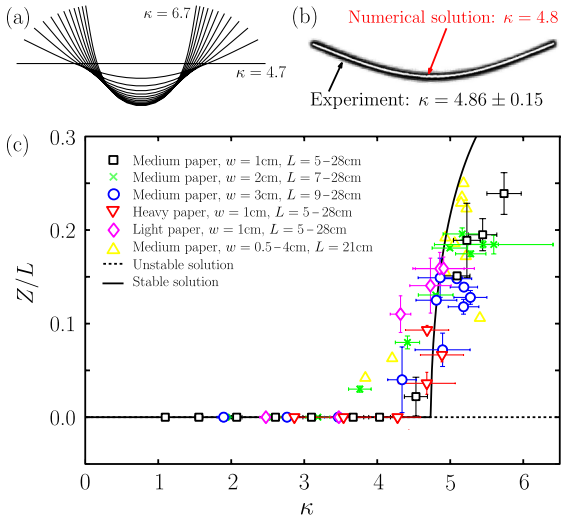

FIG. 2 (color online). (a) Computed wing shapes for $\kappa = 4.7$–6.7. (b) Front view of a tumbling, bent wing superimposed with the shape computed numerically (white line). (c) Maximum wing deflection as a function of the dimensionless parameter $\kappa = \sqrt[4]{\rho_s A \dot{\alpha}^2 / EI} L$, experiments, and theory (solid curve).

$\kappa_\star \approx 4.73$, in close agreement with our numerical results. It bears emphasis that this agreement is not due to fitting, as there are no free parameters: each parameter is obtained from direct experimental measurement. Moreover, wing shapes observed experimentally are compared with those computed numerically [11], and found to be in good agreement [Fig. 2(b)].

We now focus on flight properties of tumbling flexible wings, specifically the effect of elastic bending on flight range and descent rate. A reduced model for the flight dynamics of flexible tumbling wings is developed, which consists of coupled aeroelastic equations of motion derived in nondimensional form using the characteristic quantities $L_{\text{ref}} = w$, $m_{\text{ref}} = \rho_s AL$, $U_{\text{ref}} = \sqrt{\rho_s hg/\rho}$, and $t_{\text{ref}} = L_{\text{ref}}/U_{\text{ref}}$, where U_{ref} is a characteristic settling speed found by balancing gravity and aerodynamic forces. In the following, all equations are written in nondimensional form, and $\Lambda = L/L_{\text{ref}}$ is the nondimensional wing length.

We first derive a reduced equation for the bending dynamics of the wing. In nondimensional form, Eq. (1) becomes $\ddot{\zeta} + \Omega^2 \zeta_{ssss} - \dot{\alpha}^2 \zeta = 0$, where $\Omega = \sqrt{EI/\rho_s A} t_{\text{ref}}/L_{\text{ref}}^2$ represents a nondimensional frequency of oscillation. Substituting the solution to the linearized equations (3) for ζ yields an equation in Z only

$$\ddot{Z} + [\omega(\Lambda)^2 - \dot{\alpha}^2] Z = 0. \tag{4}$$

This reduced equation (4) describes the dynamics of a harmonic oscillator of natural frequency $\omega(\Lambda) = \Omega \kappa_\star^2 / \Lambda^2$ under inertial forcing $\dot{\alpha}^2 Z$. As expected, ω also corresponds to the lowest natural frequency for bending oscillations of a free wing. Equation (4) captures the essential physics of the inertial buckling transition. The straight wing $Z = 0$ is always a solution, but is only stable for short wings or low rotation rates for which $\omega(\Lambda) > \dot{\alpha}$. The transition occurs for $\omega(\Lambda) = \dot{\alpha}$, which corresponds precisely to Eq. (2). In this case, Z need not be zero and solutions with finite bending are possible.

We proceed by deriving the conservation equations governing the falling motion of the wing. Similar equations have been derived for rigid wings [4–6], but these studies were aimed at characterizing the fluttering-tumbling transition, while we here only consider tumbling far from the transition and investigate the first order effect of bending. The local lift $\mathbf{L}$ is proportional to the circulation around the wing Γ, as predicted by quasisteady potential flow theory, and Γ is assumed to depend only on the rotation rate $\Gamma = C_R \dot{\alpha}$, with C_R a nondimensional parameter. The local drag $\mathbf{D}$ is taken to be quadratic in the local velocity $U(s)$ with constant drag coefficient C_D. Both local lift and drag depend on the local velocity and thus on the deflection ζ. Linear momentum conservation for the entire wing is expressed in the $(\hat{\mathbf{x}}', \hat{\mathbf{z}}')$ frame by integrating the local lift, drag, and gravitational forces along the wing:

$$I_0(\dot{u} - \dot{\alpha} v) = -C_R \dot{\alpha} v - C_D U_G u - \sin\alpha, \tag{5}$$

$$I_0(\dot{v} + \dot{\alpha} u) = +C_R \dot{\alpha} u - C_D U_G v - \cos\alpha. \tag{6}$$

u and v are the components of $\mathbf{U}_G$ in the $(\hat{\mathbf{x}}', \hat{\mathbf{z}}')$ frame of reference and $I_0 = \rho_s h/\rho w$. It bears emphasis that Eqs. (5) and (6) are independent of the deflection ζ to first order. This is because ζ is taken from the center of gravity G and by definition we have $\int_{-\Lambda/2}^{\Lambda/2} \zeta(s) ds = 0$; hence any first order correction of the local forces in ζ integrates to zero.

Angular momentum conservation is expressed with respect to G. The only torque acting on the wing is the aerodynamic torque, which we decompose as the sum of an entrainment torque that causes the wing to rotate and a dissipative torque that opposes its rotation. For a straight wing, the entrainment torque is taken to be proportional to the lift, as is the case in potential flow theory, and the dissipative torque to be quadratic in $\dot{\alpha}$. For a bent wing, we must include the contribution from the moments of the aerodynamic forces about G, $\int_{-\Lambda/2}^{\Lambda/2} [\zeta \hat{\mathbf{z}}' \times (\mathbf{L} + \mathbf{D})] ds$. Here, first order corrections in ζ to $\mathbf{L}$ and $\mathbf{D}$ make nonzero contributions, which correspond to an additional term in the dissipative torque proportional to $\int_{-\Lambda/2}^{\Lambda/2} \zeta(s)^2 ds$. Substituting Eq. (3) for ζ yields a quadratic term in the total deflection Z. Hence

$$\frac{d}{dt}(J\dot{\alpha}) = \eta \dot{\alpha} U_G - \mu_1 \dot{\alpha}^2 - \mu_2 Z^2 \dot{\alpha} U_G, \tag{7}$$

where J is the nondimensional moment of inertia at G about the axis $\hat{\mathbf{y}}$, and η, μ_1, μ_2 are nondimensional aerodynamic parameters.

It is remarkable that the system of coupled nonlinear ODEs (4)–(7) has a particular solution for which the deflection Z and rotation rate $\dot{\alpha}$ remain constant throughout the motion, in agreement with our experimental observa-

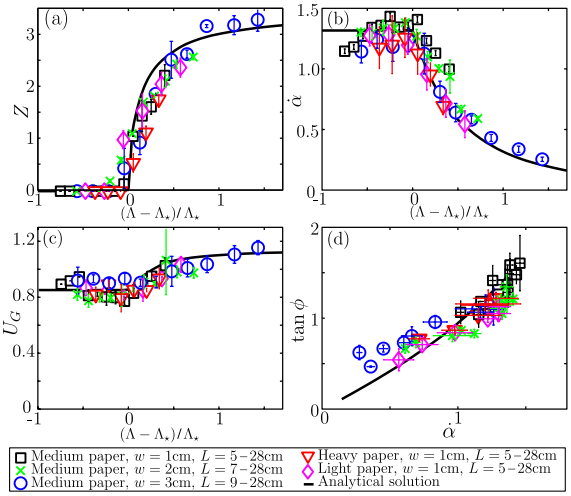

FIG. 3 (color online). Comparison between the analytical solution to our reduced model for the flight dynamics of flexible tumbling wings and experimental data of measured (a) total deflection Z, (b) linear velocity U_G, and (c) rotation rate $\dot{\alpha}$ of the wing as a function of $\Lambda/\Lambda_\star$. Figure (d) represents the angle of descent $\tan\phi$ as a function of $\dot{\alpha}$.

tions. For this solution, the ODEs (4)–(7) reduce to algebraic equations for Z, $\dot{\alpha}$, and $\mathbf{U}_G$, which may be solved analytically. Note that we are mostly interested in $\mathbf{U}_G$ since its magnitude U_G and direction from the vertical ϕ fully characterize the descent rate and range of the wing. The analytic solution can be found in [11], and depends only on the nondimensional length Λ, and four constant aerodynamic parameters C_D, C_R, η/μ_1, μ_2/μ_1. Figure 3 shows the collapse of our nondimensional experimental data for Z, $\dot{\alpha}$, U_G, ϕ as functions of Λ, and the agreement with our analytical solution. The aerodynamic parameters are chosen to best match the experimental data and all take reasonable values [11] in agreement with previous studies [6]. For example, the inferred value for C_D is 0.78, lying, as expected, between the values $C_D \approx 0$ and 2 appropriate for a wing falling, respectively, parallel and perpendicular to its cord direction.

For a short wing, before the transition, no bending occurs; hence $Z = 0$ [Fig. 3(a)]. In this regime, the analytical solutions for $\dot{\alpha}$, U_G, and ϕ are constants, independent of Λ, in accord with our experimental observations and previous studies [8]. Moreover, the collapse of the nondimensionalized experimental data confirms that, before the transition, the flight characteristics $\dot{\alpha}_\star$, $U_{G_\star}$, and $\phi_\star$ are independent of the cross-sectional geometry, which implies that the dimensional rotation rate scales with $1/t_{\mathrm{ref}} \sim h^{1/2}w^{-1}$, as suggested in [8].

The transition parameter κ increases with Λ and the buckling transition occurs when $\Lambda = \Lambda_\star = \kappa_\star\sqrt{\Omega/\dot{\alpha}_\star}$. After the transition, Z, $\dot{\alpha}$, U_G, and ϕ only depend on $\Lambda/\Lambda_\star$ and on the aerodynamic parameters. The solution can be expanded in $\Lambda/\Lambda_\star$ both around the critical point and in the limit of long wings. At the transition, the deflection Z increases sharply as the square root of the length but tends to an asymptotic value for long wings [Fig. 3(a)]. The increased Z deflection causes the wing to rotate at a smaller rate, which confirms the main effect of bending on the aerodynamics, namely, an increased dissipative torque that opposes rotation. This decrease in $\dot{\alpha}$ is first linear at the transition and goes to zero asymptotically for long wings [Fig. 3(b)]. On the other hand, the velocity U_G increases slightly before reaching an asymptotic value. While moderate, the increase is confirmed by our experimental data [Fig. 3(c)] and implies a small increase in the descent rate. Finally, the angle of descent ϕ asymptotically decays to zero [Fig. 3(d)], corresponding to a decreased range.

Our study has rationalized an abrupt change in the flight characteristics of rectangular flexible wings that accompanies their buckling transition, and so highlights the dramatic influence of elasticity on passive flight. For tumbling wings, flexibility leads to diminished flight characteristics, namely, an increased descent rate and decreased range. This trend suggests a trade-off: while a lighter wing will have greater descent times, it may suffer a buckling instability, which may diminish its flight characteristics. In the context of plant colonization, this conclusion is corroborated by the form of the tumbling seed pods of *Ailanthus altissima*. We measured their surface density, length $L \approx 5$ cm, width $w \approx 0.5$ cm, thickness $h \approx 10$ μm, and rotation rate. Estimating κ for the equivalent rectangular wing yields $\kappa \approx 5$, comparable to the critical value for buckling. Nevertheless, these tumbling seed pods are never observed to buckle, presumably owing to the chiral shape of the seedpod, which increases the bending stiffness and so represents a novel example of plant adaptation to aeroelastic constraints.

The work at Clark University was supported by the NSF under Grant No. DMR-0605664.

*dan_tam@math.mit.edu

[1] R. Nathan *et al.*, Nature (London) **418**, 409 (2002).
[2] S. Minamia and A. Azuma, J. Theor. Biol. **225**, 1 (2003).
[3] J. C. Maxwell, Camb. Dublin Math. J. **9**, 145 (1854).
[4] L. Mahadevan, C.R. Acad. Sci., Ser. IIb: Mec., Phys., Chim., Astron. **323**, 729 (1996).
[5] A. Belmonte, H. Eisenberg, and E. Moses, Phys. Rev. Lett. **81**, 345 (1998).
[6] A. Andersen, U. Pesavento, and Z. Wang, J. Fluid Mech. **541**, 91 (2005).
[7] P. Dupleich, NACA Tech. Memo. **1201**, 1 (1941).
[8] L. Mahadevan, W. Ryu, and A. Samuel, Phys. Fluids **11**, 1 (1999).
[9] T. M. Atanackovic, *Stability Theory of Elastic Rods* (World Scientific, Singapore, 1997).
[10] S. Timoshenko and J. Gere, *Theory of Elastic Stability* (McGraw-Hill, New York, 1961).
[11] See supplementary material and videos at http://link.aps.org/supplemental/10.1103/PhysRevLett.104.184504.